

Fully Relativistic Treatment of Extreme Mass-Ratio Inspirals in Collisionless Environments

Rodrigo Vicente,^{1,*} Theophanes K. Karydas,¹ and Gianfranco Bertone¹

¹*Gravitation Astroparticle Physics Amsterdam (GRAPPA),
University of Amsterdam, 1098 XH Amsterdam, The Netherlands*

(Dated: November 11, 2025)

Future mHz gravitational wave (GW) interferometers will precisely probe massive black hole environments, such as accretion disks, cold dark matter overdensities, and clouds of ultralight bosons, as long as we can accurately model the dephasing they induce on the waveform of extreme mass-ratio inspirals (EMRIs). Most existing models rely on extrapolations from Newtonian results to model the interaction of the small black hole in an EMRI system with the environment surrounding the massive black hole. Here, we present a fully relativistic formalism to model such interaction with collisionless environments, focusing on the case of cold dark matter overdensities, like “spikes” and “mounds”. We implement our new formalism in the **FastEMRIWaveforms** framework, and show that the resulting waveforms are significantly different from those based on a Newtonian treatment of environmental effects. Our results indicate that a fully relativistic treatment is essential to capture the environmental dephasing of GW signals from EMRIs accurately.

Introduction.— Next-generation GW detectors like LISA [1], TianQin [2], and DECIGO [3] will allow us to probe the environments where compact binaries form, evolve, and merge [4–8]. In particular, these mHz detectors will allow us to track individual extreme mass-ratio inspirals (EMRIs) over hundreds of thousands of orbital cycles, spanning months to years, opening up new opportunities for astrophysics [9–25] and fundamental physics [26–53]. The scientific potential of EMRIs hinges critically on the accuracy of their theoretical modeling. While these systems are inherently relativistic [54], their interactions with surrounding matter are often approximated using Newtonian extrapolations, sometimes supplemented by special relativity corrections (e.g., [55–57]); a few notable exceptions are, e.g., [25, 58, 59] for accretion disks, [35, 43, 44] for ultralight bosons, and [60] for non-gravitational forces. The inaccurate modeling of environmental effects might lead to false violations of general relativity [61], systematic biases [22], or, in extreme cases, to missing signals [22].

In this Letter, we develop a relativistic framework to model environmental effects on EMRIs in collisionless media. We then focus on dark matter (DM) spikes as a key example, assessing the significance of relativistic effects in such systems. Our results demonstrate that a fully relativistic treatment is necessary to accurately model these interactions. We adopt geometric units ($c = G = 1$) and use the mostly positive metric signature. The symbol \equiv denotes evaluation in a particular frame.

Adiabatic evolution.— The adiabatic modeling of EMRIs [54, 62] relies on a two-timescale expansion [63, 64], which separates the short orbital timescale, $T_{\text{orb}} \sim M$, over which dissipative effects are evaluated, from the long radiation-reaction timescale, $T_{\text{rad}} \sim M/q$, over which the orbit evolves; here, M is the mass of the primary black hole (BH), and $q \equiv m/M \ll 1$ is the system’s

mass ratio. In this framework, the system is described by a sequence of geodesics evolving at a rate determined by the orbit-averaged dissipative fluxes of GW radiation. The adiabatic approximation is equivalent to the leading-order dissipative effects of the first-order gravitational self-force [65, 66], neglecting conservative effects and (averaged-out) higher-order dissipative effects [67].

We build on this to develop a relativistic formalism to account for the effects of collisionless environments on EMRIs at adiabatic order (similarly to the approach taken in [54] for clouds of ultralight scalars). We consider a background spacetime described by the Kerr metric, neglecting the gravitational backreaction of the environment, which is tiny around EMRIs for most astrophysical systems, as both the enclosed mass within the orbit and the environment’s compactness are minuscule (more on that later). A geodesic ξ , with four-velocity $\mathbf{u} \equiv d\xi/d\tau$ and proper time τ , is uniquely determined by its energy, angular momentum around the axis of symmetry (i.e. the primary’s spin axis), and Carter’s constant defined by¹

$$\varepsilon \equiv -\mathbf{u} \cdot \partial_t, \quad l_z \equiv \mathbf{u} \cdot \partial_\varphi, \quad C \equiv K(\mathbf{u}, \mathbf{u}), \quad (1)$$

here normalized by the companion’s rest mass, where ∂_t and ∂_φ are, respectively, the timelike and the azimuthal Killing vectors of Kerr, and $K(\cdot, \cdot)$ is a second order Killing tensor of Kerr defined as in [68].

The flux of GW radiation to infinity and down the primary’s event horizon can be computed by solving the Teukolsky equation, as detailed in [69–71]. Their contribution to the secular evolution of the energy and angular momentum along the primary’s spin can be found directly from global conservation laws and, while more

¹ To completely fix the geodesic a point $\xi(\tau_0)$ must be supplemented.

indirectly, the evolution of the Carter’s constant can also be determined by similar techniques [62, 72–74]. A four-acceleration \mathbf{a} defined over ξ describing the interaction of the companion with a local environment results in the additional contribution

$$\dot{\epsilon}_e = -u^t \mathbf{a} \cdot \partial_t, \quad \dot{l}_{z,e} = u^t \mathbf{a} \cdot \partial_\varphi, \quad \dot{C}_e \equiv 2u^t K(\mathbf{a}, \mathbf{u}), \quad (2)$$

where the dot denotes the derivative with respect to the Boyer-Lindquist time t . These, together with the contribution of the GW fluxes, can then be orbit-averaged to compute the adiabatic evolution of the EMRI. The key question is then: how to compute the four-acceleration from a (local) interaction with an environment within general relativity?

Collisionless environment.— We consider a kinetically supported collisionless medium, under the gravitational influence of a supermassive BH—this could be, for instance, a cold DM overdensity [75–78] or a radiatively inefficient accretion disk [79–81]. Such media is described by a distribution function $F(x, \mathbf{p})$, representing the invariant number dN of particles contained in a spacelike volume element dV at x , and whose four-momenta \mathbf{p} lie within the corresponding mass-shell three-surface element dP in momentum space, which is constrained by $\mathbf{p} \cdot \mathbf{p} = -\mu^2$, with μ the rest mass of the particles. This distribution function is independent of dV , when defined through $dN \equiv F(x, \mathbf{p})(-\mathbf{p} \cdot \mathbf{n})dVdP$, where \mathbf{n} is the future timelike unit normal to dV [82]. In the following, it will be convenient to introduce (local) normal coordinates at x associated to the orthonormal frame $(\mathbf{u}, \mathbf{e}_a)$. In the induced coordinates in momentum space, the volume element is $dP = (1/p^0) dp^1 dp^2 dp^3$.

From Jeans’ theorem [83], the distribution function of a steady-state, collisionless system depends on the phase-space coordinates only through the integrals of motion. Assuming a relaxed steady-state environment, we take $F(x, \mathbf{p}) = \mu^{-3} f(\mathcal{E}, \mathcal{C}, \mathcal{L}_z)$, where $\mathcal{E}(x, \mathbf{p})$, $\mathcal{C}(x, \mathbf{p})$, and $\mathcal{L}_z(x, \mathbf{p})$ are, respectively, the energy, angular momentum along the axis of symmetry, and Carter’s constant of the environment particles, normalized by their rest mass μ .

The number of particles per phase-space volume in the companion’s local plane of simultaneity (i.e., $\mathbf{n} = \mathbf{u}$) is

$$\frac{dN}{dV d^3 v^i} \stackrel{*}{=} \gamma_v^5 f(\mathcal{E}, \mathcal{C}, \mathcal{L}_z), \quad (3)$$

where, for later convenience, we changed coordinates in the momentum space to v^a , defined by $p^a \stackrel{*}{=} \mu \gamma_v v^a$, with $\gamma_v \equiv (1 - v^2)^{-1/2}$ and $v \equiv (v^a v_a)^{1/2}$. The function $f(\mathcal{E}, \mathcal{C}, \mathcal{L}_z)$ depends on the type of environment and its evolution history, and can, in certain cases, be derived from first principles. At each position x , it is straightforward to relate \mathcal{E} , \mathcal{C} , and \mathcal{L}_z to v^i , fixing the spatial frame vectors as $\mathbf{e}_1 \propto (\partial_r + u_r \mathbf{u})$, $\mathbf{e}_2 \propto (\partial_\theta + u_\theta \mathbf{u})$, and $\mathbf{e}_3 \propto (\partial_\varphi + u_\varphi \mathbf{u})$, where (r, θ, φ) are Boyer-Lindquist

coordinates. The explicit expressions for quasi-circular EMRIs in Schwarzschild are given in the *End Matter*.

Interaction with environment.— In Fermi normal coordinates (τ, x^a) adapted to $\xi(I)$, with $I \equiv (\tau_1, \tau_1 + \delta\tau)$, the tidal field from the primary BH vanishes at leading order in a neighborhood around $\xi(I)$ [84]. Even so, when we “zoom in” close enough to the secondary object, its gravitational degrees of freedom become noticeable—this is often called the *body zone* [66]; we expect the linear size of this region to be roughly of the order of the Hill radius, i.e., $x \lesssim x_H \equiv R(q/3)^{1/3}$, for a circular orbit of radius R and a mass-ratio $q \equiv m/M \ll 1$. The extreme mass-ratio condition is crucial to establishing the separation of scales of the problem, which we will now explore.

For EMRIs immersed in incoherent collisionless media, we expect most of the energy-momentum exchange to happen locally inside the companion’s body zone. Here, we will consider the companion to be a non-spinning BH interacting with the environment through gravity, but spin effects (e.g., [85, 86]) or extra couplings to matter may be added to our framework. In the body zone, the metric is well approximated by the Schwarzschild background (here in isotropic coordinates approaching asymptotically the Fermi normal coordinates)²

$$ds^2 \approx \frac{(2\bar{r} - m)^2}{(2\bar{r} + m)^2} d\tau^2 - \left(1 + \frac{m}{2\bar{r}}\right)^4 \delta_{ab} dx^a dx^b \quad (4)$$

with $\bar{r} \equiv (\delta_{ab} x^a x^b)^{1/2}$.

The four-acceleration arising from the gravitational interaction with the environment is (by definition)

$$\mathbf{a} \equiv \nabla_{\mathbf{u}} \mathbf{u} = \frac{1}{m} \left[\nabla_{\mathbf{u}} (m\mathbf{u}) - \frac{dm}{d\tau} \mathbf{u} \right]. \quad (5)$$

The last expression can be easily evaluated in Fermi normal coordinates, using known results for particles scattering off a Schwarzschild BH. The linear momentum exchange is (in Fermi normal coordinates)

$$\mathbf{a} \stackrel{*}{=} \frac{1}{m} \int \frac{dN}{dV d^3 v^i} v [\sigma_{\text{acc}}(v) + \sigma_{\text{scat}}(v)] \mathbf{p}_\perp d^3 v^i, \quad (6)$$

with $\mathbf{p}_\perp \stackrel{*}{=} \mu \gamma_v (0, v^a)$, $dN/(dV d^3 v^i)$ as in (3), and σ_{acc} and σ_{scat} , respectively, the accretion (acc) and gravitational scattering (scat) cross sections. In the last expression, we used the isotropy of Schwarzschild.³ The integral in $dv^3 \equiv dv^1 dv^2 dv^3$ will generally have to be performed numerically.

² We assume that the four-acceleration is small enough that its effects are negligible in the body zone.

³ The companion’s spin (or asphericity) will increase the complexity of the problem, but does not pose an obstacle to our approach.

The acceleration computed in Fermi normal coordinates adapted to the companion has then to be related to the rate of change of the conserved quantities describing its motion. Explicit expressions for quasi-circular EMRIs in Schwarzschild are given in the *End Matter*.

Cold dark matter overdensity.— For concreteness, we focus on EMRIs in the presence of cold and collisionless DM. The density and velocity distribution of DM particles around BHs has been extensively discussed in the literature (see [6] for a recent review). If BHs grow adiabatically from an infinitesimal seed at the center of a DM halo with a power law density profile, DM is expected to develop a dense DM “spike” characterized by a density profile which is again a power law, but with a steeper slope [75, 87]. In practice, the finite mass and size of BH seeds imply that within a radius equal to the size of the star that eventually collapses to the BH seed, the DM distribution is predicted to form an overdensity shallower than a DM spike, referred to as DM “mound” [78]. A fully relativistic treatment of the evolution of the DM distribution function also leads to a substantial deviation of the DM density profile from the case of a Newtonian DM spike, both in the case of a Schwarzschild [76] and a Kerr BH [77].

We consider a relativistic DM spike around a massive Schwarzschild BH, and derive the distribution $f(\mathcal{E}, \mathcal{C}, \mathcal{L}_z)$ from adiabatic invariants as in [76].⁴ We consider a Milky-Way-like galaxy, assuming an isotropic host DM halo described by a Hernquist density profile [88] with mass $M_h = 10^{12} M_\odot$ and scale length $a = 20$ kpc, and a supermassive BH with mass $M = 10^6 M_\odot$. The resulting DM spike profile has a peak rest mass density of 2.4×10^{19} GeV/cm³ at $r \approx 7.7M$, as measured by stationary observers with four-velocity $\mathbf{n} = (-g_{tt})^{-1/2} \partial_t$; this scales approximately with $\propto M^{-1.7}$ (e.g., [56]).

Particle dark matter.— The process of collisionless DM scattering off a Schwarzschild BH companion is determined completely by the spacetime geodesic structure. As shown in App. B of [89], the cross sections in (6) are $\sigma_{\text{acc}} = \pi b_{\text{cr}}^2(v)$ and $\sigma_{\text{scat}} = 2\pi \int_{b > b_{\text{cr}}} db b [m \cos[\phi_\infty(b, v)] / b_{\text{gr}}(v)]^2$, where $b_{\text{gr}} \equiv (m/v^2)(1 + v^2)$ and the critical (capture) impact parameter, b_{cr} , is expressed analytically in [89]. The asymptotic true anomaly ϕ_∞ can be expressed in terms of elliptic integrals of the first kind [89, 90].

The scattering cross section can be made more explicit by expressing $\sigma_{\text{scat}} \equiv 4\pi \Lambda b_{\text{gr}}^2$, introducing the Coulomb logarithm (using an infrared cutoff $b_{\text{max}} \sim x_H$)

$$\Lambda(v) = \ln \sqrt{\frac{b_{\text{max}}^2 + b_{\text{gr}}^2(v)}{b_{\text{cr}}^2(v) + b_{\text{gr}}^2(v)}} + \chi(v),$$

⁴ As noted in footnote 3 of [77], there is a $(1 - 2M/r)^{-1}$ factor missing in the Schwarzschild’s radial invariant in Eq. (3.19) of [76].

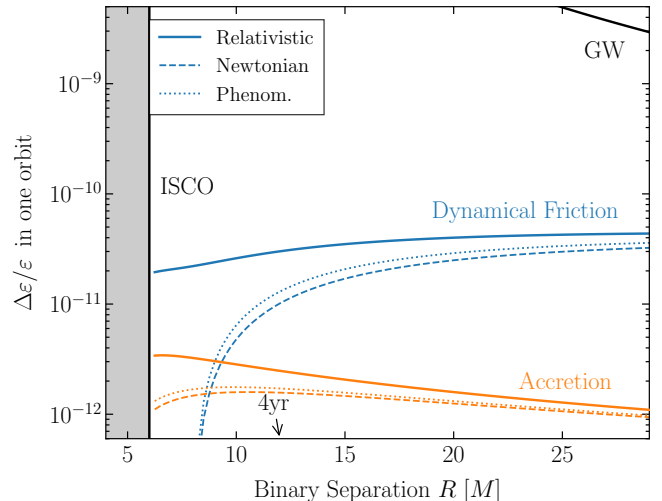


FIG. 1. **Energy loss per orbital cycle as a function of binary separation.** Solid lines correspond to the fully relativistic model, the dashed to the Newtonian, and the dotted to including heuristic relativistic corrections as in [56], for an EMRI with mass-ratio $q = 10^{-5}$ in a DM spike of a Milky-Way-like galaxy. An EMRI at $R = 12M$ will merge after ~ 4 years.

which includes the relativistic contribution

$$\chi \equiv \ln \sqrt{\frac{b_{\text{cr}}^2(v) + b_{\text{gr}}^2(v)}{b_{\text{min}}^2 + b_{\text{gr}}^2(v)}} + b_{\text{gr}}^{-2}(v) \int_{b_{\text{cr}}(v)}^{b_{\text{min}}} \cos^2[\phi_\infty(b, v)] b db,$$

where b_{min} is chosen freely, provided $b_{\text{cr}} \ll b_{\text{min}} \leq b_{\text{max}}$. The function χ is monotonically increasing and $O(1)$ for $v \gtrsim 10^{-1}$. It is accurately approximated by a simple analytic expression given in the Supplemental Material [91].

Figure 1 shows the fractional energy loss during an orbit, with $\Delta\varepsilon = \dot{\varepsilon} (2\pi/\Omega)$, due to momentum accretion, dynamical friction (elastic scattering), and gravitational wave radiation as a function of the binary separation R , computed through (8) by numerically integrating over the velocity space in (6) and using $b_{\text{max}} = x_H$. We compare the results against a Newtonian model of the environmental effects and one including phenomenological relativistic corrections as in [56]. The curves show that both models largely underestimate dynamical friction.

In both models, we keep the relativistic expressions (7) in the distribution function, to preserve the loss cone of the DM distribution; a Newtonian modeling of the loss cone would result in a depleted region $r < 8M$ [75] (as opposed to the actual $r < 4M$ [76]). We also keep $b_{\text{cr}}(v)$ to compute the effect of accretion, despite that gravitational capture is a relativistic effect. We neglect the relativistic factors γ_v in the incoming momentum \mathbf{p}_\perp , $(1 + v^2)$ in the scattering impact parameter b_{gr} , χ in the Coulomb logarithm Λ , the strong-field terms in the specific torque in (8), and use $dN/(dV d^3v^i)$ as measured by the stationary observers [$\mathbf{n} = (-g_{tt})^{-1/2} \partial_t$] in the integration (6). The latter (multiplied by the rest mass μ) coincides with the

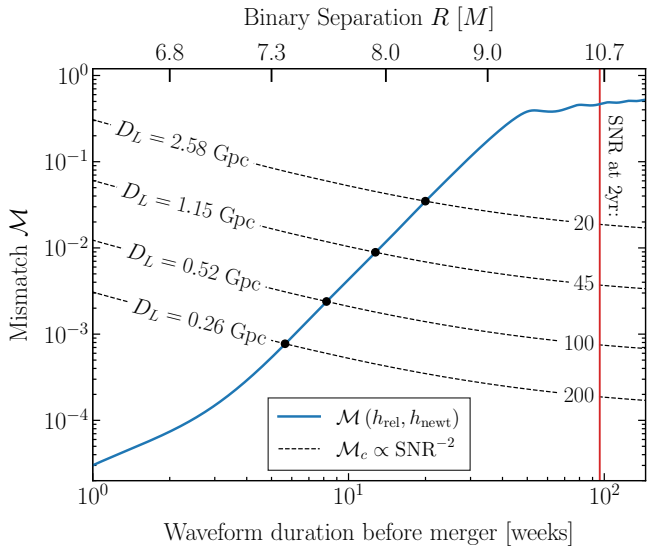


FIG. 2. **Mismatch between relativistic and Newtonian environmental models as a function of observation time (in weeks before merger).** Dashed lines mark the mismatch thresholds for various luminosity distances D_L , above which the Newtonian environmental waveform diverges significantly from the actual relativistic one, introducing systematics into LISA measurements. For an EMRI with mass-ratio $q = 10^{-5}$ embedded in a dark-matter spike of a Milky-Way-like galaxy, the mismatch exceeds the critical threshold after only a few weeks of observation.

mass density obtained in [76], which has been used in previous models of environmental effects.

For comparison, we also consider a phenomenological model of the relativistic corrections motivated by [56] (labeled “Phenom.”). This includes a multiplicative factor $\gamma_u^2 \equiv 1/(1 - u^2)$, with $u \equiv \Omega R$, to the dynamical friction and accretion torques, as an attempt to account for the volume contraction and the relativistic correction to the particles momentum from the companion’s perspective, and also a multiplicative factor $(1 + u^2)^2$ to the dynamical friction torque, from relativistic corrections to b_{gr}^2 (cf. previous paragraph). The deviation from the fully relativistic model (shown in Fig. 2) arises from neglecting strong-field effects of both the supermassive and companion BHs, and from considering the (heuristic) relativistic corrections out of the integral over the velocity space (6) (see Supplemental Material [91]).

Impact of relativistic effects.— We quantify the difference between two waveform-modeling frameworks using the “faithfulness” integral $\mathcal{F} \equiv \langle a|b \rangle / (\rho_a \rho_b)$ [92] and its complement, the “mismatch” $\mathcal{M} = 1 - \mathcal{F}$, where the noise-weighted inner product between two real waveforms $a(t)$ and $b(t)$ is given in frequency domain by the usual form (e.g., [93, Eq. (2.3)]), with the one-sided LISA power-spectral density taken to be the numerical Michelson-like PSD from [94], and $\rho_a \equiv \sqrt{\langle a|a \rangle}$ is the optimal signal-to-

noise-ratio (SNR). We evaluate the noise-weighted inner product from $f_{\text{min}} = 10^{-5}$ Hz up to the Nyquist frequency $f_{\text{max}} = 0.05$ Hz, and maximize the result over phase and time offsets as in [32]. We obtain the EMRI waveforms in each case by incorporating Eqs. 8 into the `FastEMRIWaveforms_v1.5.4` (FEW) framework [95–98], initializing binaries 4 yr before merger.

Figure 2 characterizes the importance of relativistic effects in the modeling of environmental effects in terms of what future mHz interferometers like LISA can discern. The ability of the detector to distinguish two waveforms grows with the observation time as the SNR accumulates. In particular, one can estimate the critical mismatch above which two waveforms can be distinguished in the detector by $\mathcal{M}_c = (n/2) \text{SNR}^{-2}$ [99], where n is the number of intrinsic parameters (here, equal to 15). The critical mismatch is shown in Fig. 2 as a function of the observation time for different luminosity distances (or optimal SNR at 2 yr of observation). For periods of observation with $\mathcal{M} > \mathcal{M}_c$, the relativistic effects must be included in the modeling of environmental effects to avoid systematic biases or risk a substantial loss in SNR. As a reference, for our benchmark system with $q = 10^{-5}$, this observation period falls roughly between 1 and 4.5 months for luminosity distances $D_L \in (0.3, 2.6)$ Gpc. While the precise values of the mismatch between the relativistic and Newtonian models may vary with the EMRI parameters, we do not expect our qualitative conclusions to be affected.

Newtonian models largely underestimate the impact of environmental effects on EMRI waveforms. For our benchmark system with mass-ratio $q = 10^{-5}$, we verified that an observation of more than a year before merger is required for LISA to discern those models from vacuum, as opposed to the few weeks for the fully relativistic model. Our results also show that relativistic corrections to environmental effects are comparatively weaker for systems with less extreme mass ratios, which can be understood from the fact that such systems chirp faster through the strong-field region.

Discussion.— In this Letter, we introduce a fully relativistic framework to include environmental effects of collisionless environments in the evolution of EMRIs. Applying it to the case of DM spikes around massive BHs, we showed that a fully relativistic treatment is necessary to accurately describe the environmental dephasing on such signals. In this work, we neglected the effect of the EMRI on the DM overdensity. Using the Newtonian framework `HaloFeedback` [29, 100], we confirmed that an EMRI with mass-ratio $q = 10^{-5}$ would lead to tiny feedback on the DM overdensity: the evolution of the distribution function would lead to less than one cycle of dephasing in 4 yr (corresponding to $\sim 0.5\%$ of the total dephasing). We note, though, that, for LISA data analysis, post-adiabatic EMRI waveforms with errors below one radian dephasing after 4 yr are required.

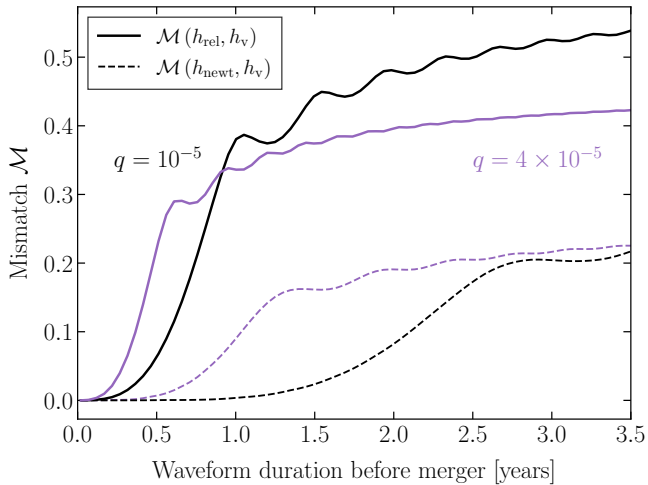


FIG. 3. **Mismatch with respect to vacuum waveforms as a function of signal duration (in years before merger).** The black and purple lines are for the benchmark ($q = 10^{-5}$), or a slightly heavier companion.

A different route to relativistic environmental effects on the generation and propagation of GWs was taken in [36] (with subsequent works [37–41]), which includes the self-gravity of surrounding matter. This was based on a result by Einstein [101], that a system of many gravitating point masses moving along circular geodesics about a common center can be mapped into an effective anisotropic fluid with only tangential pressure. Because real DM halos should contain particles distributed over a wide range of eccentricities due to processes like violent relaxation [102, 103], the physical interpretation of results derived for “Einstein clusters” should be done with care. Very rich phenomenology is observed to emerge from the coupled (linear) perturbations in the gravitational-matter sectors in such approaches. Typical halos, as our benchmark Milky-Way-like halo, have dimensionless compactness $\lesssim 10^{-6}$, leading to very small couplings between gravity and matter perturbations; it is conceivable, though, that such small effects might accumulate over the large halo scales into observable imprints in GW waveforms. In low-compactness collisionless halos, effects on GW propagation described within geometric optics approximation via a gravitational redshift [104] lead roughly to one dephasing cycle after $\sim 10^6$ cycles; this is $\sim 10^3$ times smaller than the effects of dynamical friction studied here (as found in [57]).

In this Letter, we imposed a hard cutoff on the impact parameter, (conservatively) neglecting the interactions with DM particles outside the secondary’s Hill radius, where the validity of our assumptions breaks down. We expect the total torque resulting from additional gravitational three-body interactions to increase the impact of environmental effects on EMRI evolution. Such “stirring” effect could, in principle, be obtained perturbatively by

computing the energy and angular momentum exchange with the DM particles mediated by (vacuum) linear metric perturbations, similarly to the approach of [44] to ultralight scalar fields.

Direct extensions of this work include the application of our framework to eccentric and inclined EMRIs onto a primary Kerr BH. We note that cold DM spikes can be significantly denser around spinning BHs [77]. Moreover, we expect relativistic effects in the interaction of EMRIs with environments to be even more important for prograde orbits around highly spinning BHs, as their ISCO (and marginally bound orbits) approaches the event horizon radius. Here, we neglected the spin of the secondary, but the results of [85] could be directly incorporated into our framework. Surrounding environments are responsible for a characteristic coevolution of the mass and spin of the companion (explored in [105]); while unmeasurable for quasicircular EMRIs [106], the spin of the companion might be probed with eccentricity [107].

Acknowledgments.— We thank Francisco Duque and Lorenzo Speri for valuable discussions and guidance on implementing our results in FEW. We are also grateful to Miguel R. Correia for insightful conversations in the early stages of this work. We also thank Emanuele Berti, Vitor Cardoso, Francisco Duque, Andrea Maselli, and Nick Speeney for their helpful comments and stimulating discussions on our draft. We gratefully acknowledge the support of the Dutch Research Council (NWO) through an Open Competition Domain Science-M grant, project number OCENW.M.21.375.

* r.l.lourencovicente@uva.nl

- [1] K. G. Arun *et al.* (LISA), New horizons for fundamental physics with LISA, *Living Rev. Rel.* **25**, 4 (2022), [arXiv:2205.01597](https://arxiv.org/abs/2205.01597) [gr-qc].
- [2] J. Luo *et al.* (TianQin), TianQin: a space-borne gravitational wave detector, *Class. Quant. Grav.* **33**, 035010 (2016), [arXiv:1512.02076](https://arxiv.org/abs/1512.02076) [astro-ph.IM].
- [3] S. Kawamura *et al.*, Current status of space gravitational wave antenna DECIGO and B-DECIGO, *PTEP* **2021**, 05A105 (2021), [arXiv:2006.13545](https://arxiv.org/abs/2006.13545) [gr-qc].
- [4] V. Cardoso and A. Maselli, Constraints on the astrophysical environment of binaries with gravitational-wave observations, *Astron. Astrophys.* **644**, A147 (2020), [arXiv:1909.05870](https://arxiv.org/abs/1909.05870) [astro-ph.HE].
- [5] G. Caneva Santoro, S. Roy, R. Vicente, M. Haney, O. J. Piccinni, W. Del Pozzo, and M. Martinez, First Constraints on Compact Binary Environments from LIGO-Virgo Data, *Phys. Rev. Lett.* **132**, 251401 (2024), [arXiv:2309.05061](https://arxiv.org/abs/2309.05061) [gr-qc].
- [6] G. Bertone, Dark matter, black holes, and gravitational waves, *Nucl. Phys. B* **1003**, 116487 (2024), [arXiv:2404.11513](https://arxiv.org/abs/2404.11513) [astro-ph.CO].
- [7] L. Zwick, J. Takátsy, P. Saini, K. Hendriks, J. Samsing, C. Tiede, C. Rowan, and A. A. Trani, Envi-

- ronmental effects in stellar mass gravitational wave sources I: Expected fraction of signals with significant dephasing in the dynamical and AGN channels, (2025), [arXiv:2503.24084 \[astro-ph.HE\]](#).
- [8] M. Colpi *et al.* (LISA), LISA Definition Study Report, (2024), [arXiv:2402.07571 \[astro-ph.CO\]](#).
- [9] E. Barausse and L. Rezzolla, The Influence of the hydrodynamic drag from an accretion torus on extreme mass-ratio inspirals, *Phys. Rev. D* **77**, 104027 (2008), [arXiv:0711.4558 \[gr-qc\]](#).
- [10] B. Kocsis, N. Yunes, and A. Loeb, Observable Signatures of EMRI Black Hole Binaries Embedded in Thin Accretion Disks, *Phys. Rev. D* **84**, 024032 (2011), [arXiv:1104.2322 \[astro-ph.GA\]](#).
- [11] N. Yunes, B. Kocsis, A. Loeb, and Z. Haiman, Imprint of Accretion Disk-Induced Migration on Gravitational Waves from Extreme Mass Ratio Inspirals, *Phys. Rev. Lett.* **107**, 171103 (2011), [arXiv:1103.4609 \[astro-ph.CO\]](#).
- [12] E. Barausse, V. Cardoso, and P. Pani, Can environmental effects spoil precision gravitational-wave astrophysics?, *Phys. Rev. D* **89**, 104059 (2014), [arXiv:1404.7149 \[gr-qc\]](#).
- [13] N. Tamanini, A. Klein, C. Bonvin, E. Barausse, and C. Caprini, Peculiar acceleration of stellar-origin black hole binaries: Measurement and biases with LISA, *Phys. Rev. D* **101**, 063002 (2020), [arXiv:1907.02018 \[astro-ph.IM\]](#).
- [14] R. Vicente, V. Cardoso, and M. Zilhão, Dynamical friction in slab geometries and accretion disks, *Mon. Not. Roy. Astron. Soc.* **489**, 5424 (2019), [arXiv:1905.06353 \[astro-ph.GA\]](#).
- [15] A. Toubiana *et al.*, Detectable environmental effects in GW190521-like black-hole binaries with LISA, *Phys. Rev. Lett.* **126**, 101105 (2021), [arXiv:2010.06056 \[astro-ph.HE\]](#).
- [16] A. Derdzinski, D. D’Orazio, P. Duffell, Z. Haiman, and A. MacFadyen, Evolution of gas disc-embedded intermediate mass ratio inspirals in the *LISA* band, *Mon. Not. Roy. Astron. Soc.* **501**, 3540 (2021), [arXiv:2005.11333 \[astro-ph.HE\]](#).
- [17] L. Zwick, A. Derdzinski, M. Garg, P. R. Capelo, and L. Mayer, Dirty waveforms: multiband harmonic content of gas-embedded gravitational wave sources, *Mon. Not. Roy. Astron. Soc.* **511**, 6143 (2022), [arXiv:2110.09097 \[astro-ph.HE\]](#).
- [18] L. Sberna *et al.*, Observing GW190521-like binary black holes and their environment with LISA, *Phys. Rev. D* **106**, 064056 (2022), [arXiv:2205.08550 \[gr-qc\]](#).
- [19] L. Zwick, P. R. Capelo, and L. Mayer, Priorities in gravitational waveforms for future space-borne detectors: vacuum accuracy or environment?, *Mon. Not. Roy. Astron. Soc.* **521**, 4645 (2023), [arXiv:2209.04060 \[gr-qc\]](#).
- [20] A. Vijaykumar, A. Tiwari, S. J. Kapadia, K. G. Arun, and P. Ajith, Waltzing Binaries: Probing the Line-of-sight Acceleration of Merging Compact Objects with Gravitational Waves, *Astrophys. J.* **954**, 105 (2023), [arXiv:2302.09651 \[astro-ph.HE\]](#).
- [21] F. Duque, S. Kejriwal, L. Sberna, L. Speri, and J. Gair, Constraining accretion physics with gravitational waves from eccentric extreme-mass-ratio inspirals, *Phys. Rev. D* **111**, 084006 (2025), [arXiv:2411.03436 \[gr-qc\]](#).
- [22] S. Roy and R. Vicente, Compact binary coalescences in dense gaseous environments can pose as ones in vacuum, *Phys. Rev. D* **111**, 084037 (2025), [arXiv:2410.16388 \[gr-qc\]](#).
- [23] T. F. M. Spieksma and E. Cannizzaro, In the grip of the disk: dragging the companion through an AGN, (2025), [arXiv:2504.08033 \[astro-ph.GA\]](#).
- [24] L. Copparoni, E. Barausse, L. Speri, L. Sberna, and A. Derdzinski, Implications of stochastic gas torques for asymmetric binaries in the LISA band, *Phys. Rev. D* **111**, 104079 (2025), [arXiv:2502.10087 \[gr-qc\]](#).
- [25] F. Duque, L. Sberna, A. Spiers, and R. Vicente, Extreme-mass-ratio inspirals in relativistic accretion discs, (2025), [arXiv:2510.02433 \[gr-qc\]](#).
- [26] L. Barack *et al.*, Black holes, gravitational waves and fundamental physics: a roadmap, *Class. Quant. Grav.* **36**, 143001 (2019), [arXiv:1806.05195 \[gr-qc\]](#).
- [27] G. Bertone *et al.*, Gravitational wave probes of dark matter: challenges and opportunities, *SciPost Phys. Core* **3**, 007 (2020), [arXiv:1907.10610 \[astro-ph.CO\]](#).
- [28] L. Annulli, V. Cardoso, and R. Vicente, Response of ultralight dark matter to supermassive black holes and binaries, *Phys. Rev. D* **102**, 063022 (2020), [arXiv:2009.00012 \[gr-qc\]](#).
- [29] B. J. Kavanagh, D. A. Nichols, G. Bertone, and D. Gaggero, Detecting dark matter around black holes with gravitational waves: Effects of dark-matter dynamics on the gravitational waveform, *Phys. Rev. D* **102**, 083006 (2020), [arXiv:2002.12811 \[gr-qc\]](#).
- [30] D. Baumann, G. Bertone, J. Stout, and G. M. Tomaselli, Ionization of gravitational atoms, *Phys. Rev. D* **105**, 115036 (2022), [arXiv:2112.14777 \[gr-qc\]](#).
- [31] A. Maselli, N. Franchini, L. Gualtieri, T. P. Sotiriou, S. Barsanti, and P. Pani, Detecting fundamental fields with LISA observations of gravitational waves from extreme mass-ratio inspirals, *Nature Astron.* **6**, 464 (2022), [arXiv:2106.11325 \[gr-qc\]](#).
- [32] A. Coogan, G. Bertone, D. Gaggero, B. J. Kavanagh, and D. A. Nichols, Measuring the dark matter environments of black hole binaries with gravitational waves, *Phys. Rev. D* **105**, 043009 (2022), [arXiv:2108.04154 \[gr-qc\]](#).
- [33] R. Vicente and V. Cardoso, Dynamical friction of black holes in ultralight dark matter, *Phys. Rev. D* **105**, 083008 (2022), [arXiv:2201.08854 \[gr-qc\]](#).
- [34] D. Traykova, R. Vicente, K. Clough, T. Helfer, E. Berti, P. G. Ferreira, and L. Hui, Relativistic drag forces on black holes from scalar dark matter clouds of all sizes, *Phys. Rev. D* **108**, L121502 (2023), [arXiv:2305.10492 \[gr-qc\]](#).
- [35] F. Duque, C. F. B. Macedo, R. Vicente, and V. Cardoso, Extreme-Mass-Ratio Inspirals in Ultralight Dark Matter, *Phys. Rev. Lett.* **133**, 121404 (2024), [arXiv:2312.06767 \[gr-qc\]](#).
- [36] V. Cardoso, K. Destounis, F. Duque, R. P. Macedo, and A. Maselli, Black holes in galaxies: Environmental impact on gravitational-wave generation and propagation, *Phys. Rev. D* **105**, L061501 (2022), [arXiv:2109.00005 \[gr-qc\]](#).
- [37] V. Cardoso, K. Destounis, F. Duque, R. Panosso Macedo, and A. Maselli, Gravitational Waves from Extreme-Mass-Ratio Systems in Astrophysical Environments, *Phys. Rev. Lett.* **129**, 241103 (2022), [arXiv:2210.01133 \[gr-qc\]](#).
- [38] T. F. M. Spieksma, V. Cardoso, G. Carullo, M. Della Rocca, and F. Duque, Black Hole Spectroscopy in Environments: Detectability Prospects, *Phys. Rev. Lett.* **134**, 081402 (2025), [arXiv:2409.05950 \[gr-qc\]](#).
- [39] N. Speeney, E. Berti, V. Cardoso, and A. Maselli, Black holes surrounded by generic matter distributions: Polar

- perturbations and energy flux, *Phys. Rev. D* **109**, 084068 (2024), [arXiv:2401.00932 \[gr-qc\]](#).
- [40] L. Pezzella, K. Destounis, A. Maselli, and V. Cardoso, Quasinormal modes of black holes embedded in halos of matter, *Phys. Rev. D* **111**, 064026 (2025), [arXiv:2412.18651 \[gr-qc\]](#).
- [41] S. Gliorio, E. Berti, A. Maselli, and N. Speeney, Extreme mass ratio inspirals in dark matter halos: dynamics and distinguishability of halo models, (2025), [arXiv:2503.16649 \[gr-qc\]](#).
- [42] P. S. Cole, G. Bertone, A. Coogan, D. Gaggero, T. Karydas, B. J. Kavanagh, T. F. M. Spieksma, and G. M. Tomaselli, Distinguishing environmental effects on binary black hole gravitational waveforms, *Nature Astron.* **7**, 943 (2023), [arXiv:2211.01362 \[gr-qc\]](#).
- [43] R. Brito and S. Shah, Extreme mass-ratio inspirals into black holes surrounded by scalar clouds, *Phys. Rev. D* **108**, 084019 (2023), [Erratum: *Phys.Rev.D* 110, 109902 (2024)], [arXiv:2307.16093 \[gr-qc\]](#).
- [44] C. Dyson, T. F. M. Spieksma, R. Brito, M. van de Meent, and S. Dolan, Environmental effects in extreme mass ratio inspirals: perturbations to the environment in Kerr, (2025), [arXiv:2501.09806 \[gr-qc\]](#).
- [45] G. M. Tomaselli, T. F. M. Spieksma, and G. Bertone, Dynamical friction in gravitational atoms, *JCAP* **07**, 070, [arXiv:2305.15460 \[gr-qc\]](#).
- [46] S. Mitra, S. Chakraborty, R. Vicente, and J. C. Feng, Probing the quantum nature of black holes with ultralight boson environments, *Phys. Rev. D* **110**, 084012 (2024), [arXiv:2312.06783 \[gr-qc\]](#).
- [47] M. Rahman, S. Kumar, and A. Bhattacharyya, Probing astrophysical environment with eccentric extreme mass-ratio inspirals, *JCAP* **01**, 035, [arXiv:2306.14971 \[gr-qc\]](#).
- [48] T. K. Karydas, B. J. Kavanagh, and G. Bertone, Sharpening the dark matter signature in gravitational waveforms. I. Accretion and eccentricity evolution, *Phys. Rev. D* **111**, 063070 (2025), [arXiv:2402.13053 \[gr-qc\]](#).
- [49] B. J. Kavanagh, T. K. Karydas, G. Bertone, P. Di Cintio, and M. Pasquato, Sharpening the dark matter signature in gravitational waveforms. II. Numerical simulations, *Phys. Rev. D* **111**, 063071 (2025), [arXiv:2402.13762 \[gr-qc\]](#).
- [50] D. Blas, S. Gasparotto, and R. Vicente, Searching for ultralight dark matter through frequency modulation of gravitational waves, *Phys. Rev. D* **111**, 042008 (2025), [arXiv:2410.07330 \[hep-ph\]](#).
- [51] A. L. Miller, Gravitational wave probes of particle dark matter: a review, (2025), [arXiv:2503.02607 \[astro-ph.HE\]](#).
- [52] M. Bošković, F. Duque, M. C. Ferreira, F. S. Miguel, and V. Cardoso, Motion in time-periodic backgrounds with applications to ultralight dark matter haloes at galactic centers, *Phys. Rev. D* **98**, 024037 (2018), [arXiv:1806.07331 \[gr-qc\]](#).
- [53] M. Bošković, M. Koschnitzke, and R. A. Porto, Signatures of Ultralight Bosons in the Orbital Eccentricity of Binary Black Holes, *Phys. Rev. Lett.* **133**, 121401 (2024), [arXiv:2403.02415 \[gr-qc\]](#).
- [54] H. Khalvati, A. Santini, F. Duque, L. Speri, J. Gair, H. Yang, and R. Brito, Impact of relativistic waveforms in LISA's science objectives with extreme-mass-ratio inspirals, (2024), [arXiv:2410.17310 \[gr-qc\]](#).
- [55] E. Barausse, Relativistic dynamical friction in a collisional fluid, *Mon. Not. Roy. Astron. Soc.* **382**, 826 (2007), [arXiv:0709.0211 \[astro-ph\]](#).
- [56] N. Speeney, A. Antonelli, V. Baibhav, and E. Berti, Impact of relativistic corrections on the detectability of dark-matter spikes with gravitational waves, *Phys. Rev. D* **106**, 044027 (2022), [arXiv:2204.12508 \[gr-qc\]](#).
- [57] S. Mitra, N. Speeney, S. Chakraborty, and E. Berti, Extreme mass ratio inspirals in rotating dark matter spikes, (2025), [arXiv:2505.04697 \[gr-qc\]](#).
- [58] C. M. Hirata, Lindblad resonance torques in relativistic discs: I. Basic equations, *Mon. Not. Roy. Astron. Soc.* **414**, 3198 (2011), [arXiv:1010.0758 \[astro-ph.HE\]](#).
- [59] C. M. Hirata, Lindblad resonance torques in relativistic discs: II. Computation of resonance strengths, *Mon. Not. Roy. Astron. Soc.* **414**, 3212 (2011), [arXiv:1010.0759 \[astro-ph.HE\]](#).
- [60] M. Correia, Covariant formulation of relativistic mechanics, *Phys. Rev. D* **105**, 084041 (2022), [arXiv:2202.04658 \[gr-qc\]](#).
- [61] M. Garg, L. Sberna, L. Speri, F. Duque, and J. Gair, Systematics in tests of general relativity using LISA massive black hole binaries, *Mon. Not. Roy. Astron. Soc.* **535**, 3283 (2024), [arXiv:2410.02910 \[astro-ph.GA\]](#).
- [62] S. A. Hughes, S. Drasco, E. E. Flanagan, and J. Franklin, Gravitational radiation reaction and inspiral waveforms in the adiabatic limit, *Phys. Rev. Lett.* **94**, 221101 (2005), [arXiv:gr-qc/0504015](#).
- [63] T. Hinderer and E. E. Flanagan, Two timescale analysis of extreme mass ratio inspirals in Kerr. I. Orbital Motion, *Phys. Rev. D* **78**, 064028 (2008), [arXiv:0805.3337 \[gr-qc\]](#).
- [64] J. Miller and A. Pound, Two-timescale evolution of extreme-mass-ratio inspirals: waveform generation scheme for quasicircular orbits in Schwarzschild spacetime, *Phys. Rev. D* **103**, 064048 (2021), [arXiv:2006.11263 \[gr-qc\]](#).
- [65] L. Barack and A. Pound, Self-force and radiation reaction in general relativity, *Rept. Prog. Phys.* **82**, 016904 (2019), [arXiv:1805.10385 \[gr-qc\]](#).
- [66] A. Pound and B. Wardell, Black hole perturbation theory and gravitational self-force, (2021), [arXiv:2101.04592 \[gr-qc\]](#).
- [67] A. Pound, E. Poisson, and B. G. Nickel, Limitations of the adiabatic approximation to the gravitational self-force, *Phys. Rev. D* **72**, 124001 (2005), [arXiv:gr-qc/0509122](#).
- [68] R. M. Wald, *General Relativity* (Chicago Univ. Pr., Chicago, USA, 1984).
- [69] C. Cutler, D. Kennefick, and E. Poisson, Gravitational radiation reaction for bound motion around a Schwarzschild black hole, *Phys. Rev. D* **50**, 3816 (1994).
- [70] S. A. Hughes, The Evolution of circular, nonequatorial orbits of Kerr black holes due to gravitational wave emission, *Phys. Rev. D* **61**, 084004 (2000), [Erratum: *Phys.Rev.D* 63, 049902 (2001), Erratum: *Phys.Rev.D* 65, 069902 (2002), Erratum: *Phys.Rev.D* 67, 089901 (2003), Erratum: *Phys.Rev.D* 78, 109902 (2008), Erratum: *Phys.Rev.D* 90, 109904 (2014)], [arXiv:gr-qc/9910091](#).
- [71] S. Drasco and S. A. Hughes, Gravitational wave snapshots of generic extreme mass ratio inspirals, *Phys. Rev. D* **73**, 024027 (2006), [Erratum: *Phys.Rev.D* 88, 109905 (2013), Erratum: *Phys.Rev.D* 90, 109905 (2014)], [arXiv:gr-qc/0509101](#).
- [72] Y. Mino, Perturbative approach to an orbital evolution around a supermassive black hole, *Phys. Rev. D* **67**, 084027 (2003), [arXiv:gr-qc/0302075](#).

- [73] S. Drasco, E. E. Flanagan, and S. A. Hughes, Computing inspirals in Kerr in the adiabatic regime. I. The Scalar case, *Class. Quant. Grav.* **22**, S801 (2005), [arXiv:gr-qc/0505075](#).
- [74] N. Sago, T. Tanaka, W. Hikida, and H. Nakano, Adiabatic radiation reaction to the orbits in Kerr spacetime, *Prog. Theor. Phys.* **114**, 509 (2005), [arXiv:gr-qc/0506092](#).
- [75] P. Gondolo and J. Silk, Dark matter annihilation at the galactic center, *Phys. Rev. Lett.* **83**, 1719 (1999), [arXiv:astro-ph/9906391](#).
- [76] L. Sadeghian, F. Ferrer, and C. M. Will, Dark matter distributions around massive black holes: A general relativistic analysis, *Phys. Rev. D* **88**, 063522 (2013), [arXiv:1305.2619 \[astro-ph.GA\]](#).
- [77] F. Ferrer, A. M. da Rosa, and C. M. Will, Dark matter spikes in the vicinity of Kerr black holes, *Phys. Rev. D* **96**, 083014 (2017), [arXiv:1707.06302 \[astro-ph.CO\]](#).
- [78] G. Bertone, A. R. A. C. Wierda, D. Gaggero, B. J. Kavanagh, M. Volonteri, and N. Yoshida, Dark Matter Mounds: towards a realistic description of dark matter overdensities around black holes, (2024), [arXiv:2404.08731 \[astro-ph.CO\]](#).
- [79] C. Cremaschini, J. C. Miller, and M. Tassarotto, Kinetic description of quasi-stationary axisymmetric collisionless accretion disk plasmas with arbitrary magnetic field configurations, *Physics of Plasmas* **18**, 062901 (2011), [arXiv:1102.0179 \[astro-ph.HE\]](#).
- [80] M. Hoshino, Angular Momentum Transport and Particle Acceleration during Magnetorotational Instability in a Kinetic Accretion Disk, *Phys. Rev. Lett.* **114**, 061101 (2015), [arXiv:1502.02452 \[astro-ph.HE\]](#).
- [81] J. Vos, B. Cerutti, M. Moscibrodzka, and K. Parfrey, Particle Acceleration in Collisionless Magnetically Arrested Disks, (2024), [arXiv:2410.19061 \[astro-ph.HE\]](#).
- [82] R. W. Lindquist, Relativistic transport theory, *Annals Phys.* **37**, 487 (1966).
- [83] J. H. Jeans, On the theory of star-streaming and the structure of the universe, *Mon. Not. Roy. Astron. Soc.* **76**, 70 (1915).
- [84] F. K. Manasse and C. W. Misner, Fermi Normal Coordinates and Some Basic Concepts in Differential Geometry, *J. Math. Phys.* **4**, 735 (1963).
- [85] C. Dyson, J. Redondo-Yuste, M. van de Meent, and V. Cardoso, Relativistic aerodynamics of spinning black holes, *Phys. Rev. D* **109**, 104038 (2024), [arXiv:2402.07981 \[gr-qc\]](#).
- [86] Z. Wang, T. Helfer, D. Traykova, K. Clough, and E. Berti, Gravitational Magnus effect from scalar dark matter, *Phys. Rev. D* **110**, 024009 (2024), [arXiv:2402.07977 \[gr-qc\]](#).
- [87] G. D. Quinlan, L. Hernquist, and S. Sigurdsson, Models of Galaxies with Central Black Holes: Adiabatic Growth in Spherical Galaxies, *Astrophys. J.* **440**, 554 (1995), [arXiv:astro-ph/9407005](#).
- [88] L. Hernquist, An Analytical Model for Spherical Galaxies and Bulges, *Astrophys. J.* **356**, 359 (1990).
- [89] D. Traykova, R. Vicente, K. Clough, T. Helfer, E. Berti, P. G. Ferreira, and L. Hui, Relativistic drag forces on black holes from scalar dark matter clouds of all sizes, *Phys. Rev. D* **108**, L121502 (2023), [arXiv:2305.10492 \[gr-qc\]](#).
- [90] S. Chandrasekhar, *The Mathematical Theory of Black Holes*, Oxford classic texts in the physical sciences (Clarendon Press, 1998).
- [91] See Supplemental Material at [\[URL\]](#) for details.
- [92] T. Damour, B. R. Iyer, and B. S. Sathyaprakash, Improved filters for gravitational waves from inspiralling compact binaries, *Phys. Rev. D* **57**, 885 (1998), [arXiv:gr-qc/9708034](#).
- [93] C. Cutler and E. E. Flanagan, Gravitational waves from merging compact binaries: How accurately can one extract the binary's parameters from the inspiral wave form?, *Phys. Rev. D* **49**, 2658 (1994), [arXiv:gr-qc/9402014](#).
- [94] T. Robson, N. J. Cornish, and C. Liu, The construction and use of lisa sensitivity curves, *Classical and Quantum Gravity* **36**, 105011 (2019).
- [95] M. L. Katz, A. J. K. Chua, L. Speri, N. Warburton, and S. A. Hughes, Fast extreme-mass-ratio-inspiral waveforms: New tools for millihertz gravitational-wave data analysis, *Phys. Rev. D* **104**, 064047 (2021), [arXiv:2104.04582 \[gr-qc\]](#).
- [96] A. J. Chua, M. L. Katz, N. Warburton, and S. A. Hughes, Rapid generation of fully relativistic extreme-mass-ratio-inspiral waveform templates for lisa data analysis, *Physical Review Letters* **126**, 10.1103/physrevlett.126.051102 (2021).
- [97] L. Speri, M. L. Katz, A. J. K. Chua, S. A. Hughes, N. Warburton, J. E. Thompson, C. E. A. Chapman-Bird, and J. R. Gair, Fast and fourier: extreme mass ratio inspiral waveforms in the frequency domain, *Frontiers in Applied Mathematics and Statistics* **9**, 10.3389/fams.2023.1266739 (2024).
- [98] C. E. A. Chapman-Bird, L. Speri, Z. Nasipak, O. Burke, M. L. Katz, A. Santini, S. Kejriwal, P. Lynch, J. Mathews, H. Khalvati, J. E. Thompson, S. Isoyama, S. A. Hughes, N. Warburton, A. J. K. Chua, and M. Pigou, The fast and the frame-dragging: Efficient waveforms for asymmetric-mass eccentric equatorial inspirals into rapidly-spinning black holes (2025), [arXiv:2506.09470 \[gr-qc\]](#).
- [99] K. Chatziioannou, A. Klein, N. Yunes, and N. Cornish, Constructing Gravitational Waves from Generic Spin-Precessing Compact Binary Inspirals, *Phys. Rev. D* **95**, 104004 (2017), [arXiv:1703.03967 \[gr-qc\]](#).
- [100] B. J. Kavanagh, [HaloFeedback \[Code, v0.9\]](#), <https://github.com/bradkav/HaloFeedback>, DOI:10.5281/zenodo.3688813 (2020).
- [101] A. Einstein, On a stationary system with spherical symmetry consisting of many gravitating masses, *Annals Math.* **40**, 922 (1939).
- [102] D. Lynden-Bell, Statistical mechanics of violent relaxation in stellar systems, *Mon. Not. Roy. Astron. Soc.* **136**, 101 (1967).
- [103] D. N. Spergel and L. Hernquist, Statistical Mechanics of Violent Relaxation, *Astrophys. J. Lett.* **397**, L75 (1992).
- [104] P. Laguna, S. L. Larson, D. Spergel, and N. Yunes, Integrated Sachs-Wolfe Effect for Gravitational Radiation, *Astrophys. J. Lett.* **715**, L12 (2010), [arXiv:0905.1908 \[gr-qc\]](#).
- [105] T. K. Karydas, R. Vicente, and G. Bertone, Mass and spin coevolution of black holes inspiralling through dark matter, (2025), [arXiv:2510.13604 \[gr-qc\]](#).
- [106] G. A. Piovano, R. Brito, A. Maselli, and P. Pani, Assessing the detectability of the secondary spin in extreme mass-ratio inspirals with fully relativistic numerical waveforms, *Phys. Rev. D* **104**, 124019 (2021),

arXiv:2105.07083 [gr-qc].

- [107] Q. Cui, W.-B. Han, and Z. Pan, Secondary spins of extreme mass ratio inspirals: Measurement precision and astrophysical applications, (2025), arXiv:2502.00856 [astro-ph.HE].

END MATTER

Quasi-circular EMRIs in Schwarzschild.— For quasi-circular EMRIs in Schwarzschild ($r = R$, $\theta = \pi/2$, $u_\theta = u_r = 0$), the conserved quantities of the DM particles can be expressed in terms of their velocity in the companion's proper frame as

$$\begin{aligned} \frac{\mathcal{E}}{\varepsilon} &= \gamma_v \frac{1 + v_3(l_z/R)}{\sqrt{1 + (l_z/R)^2}}, & \mathcal{C}^{1/2} &= \gamma_v R |v_2|, \\ \frac{\mathcal{L}_z}{l_z} &= \gamma_v \left[1 + v_3 \sqrt{1 + (R/l_z)^2} \right], \end{aligned} \quad (7)$$

where $\varepsilon = \frac{R-2M}{\sqrt{R(R-3M)}}$ and $|l_z| = \frac{R\sqrt{M}}{\sqrt{R-3M}}$ are the companion's specific energy and angular momentum.

The rate of change of the conserved quantities of a (equatorial) quasi-circular EMRI in Schwarzschild will be [from Eqs. (2)]

$$\begin{aligned} \frac{\dot{\varepsilon}_e}{\varepsilon} &= \frac{a_3(l_z/R)}{\sqrt{1 - \frac{3M}{R}} \sqrt{1 + (l_z/R)^2}}, & \dot{\mathcal{C}}_e^{1/2} &= \frac{R|a_2|}{\sqrt{1 - \frac{3M}{R}}}, \\ \frac{\dot{l}_{z,e}}{|l_z|} &= \frac{a_3}{\sqrt{1 - \frac{3M}{R}}} \sqrt{(R/l_z)^2 + 1}, \end{aligned} \quad (8)$$

where the acceleration components are in the companion's proper frame. The orbit is maintained equatorial if a_2 (or its orbit average) vanishes. In particular, this is the case if the environment's distribution function is symmetric with respect to the equatorial plane.

Parallel transport of e_a .— The careful reader may have noticed that the frame e_a chosen in the previous section is not parallel transported along ξ . This means that, in Fermi normal coordinates, the expressions (7)—which we use to compute the integral over the distribution function in (6)—are strictly valid only at a given instant τ_1 . Nevertheless, they remain a good approximation for an interval $\delta\tau \ll R^2/|l_z|$, the timescale for the parallel transported frame to change significantly from the one we use. As the gravitational scattering happens over a very much shorter timescale $\delta\tau_{\text{int}} \lesssim (x_H/R)\sqrt{1 + (l_z/R)^2}(R^2/|l_z|) \ll (R^2/|l_z|)$,⁵ we can to a good approximation use (7) to evaluate (6).

Heuristic corrections.— In Fig. 2 we compared the energy losses from our self-consistent relativistic treatment of environmental effects in DM spikes with those from a heuristic relativistic prescription that still accounts for the DM velocity dispersion (as σ_{acc} and σ_{scat} are integrated over velocity space). The reasons for the large differences observed were discussed in the text. Here, we report that in [56] the Coulomb logarithm was fixed to the (arbitrary) constant value $\Lambda = 3$, and the velocity distribution was not taken into account when computing the acceleration; coincidentally, this results in a torque closer to our fully relativistic model.

SUPPLEMENTAL MATERIAL

Relativistic Coulomb logarithm.— In computing the momentum transferred by particles scattering off a Schwarzschild spacetime, the contribution from orbits with asymptotic velocity v and impact parameter $b \gtrsim b_{\text{cr}}(v)$ (i.e., only slightly larger than the one of capture) must be computed numerically [34]. This contribution can be encapsulated in the factor $\chi(v)$ defined in the main text. Choosing $b_{\text{min}} = 40b_{\text{cr}}(v)$, the function χ is accurately described (with an error $\leq 1.5\%$) by the fit

$$\chi \approx \ln \sqrt{\frac{b_{\text{cr}}^2(v) + b_{\text{gr}}^2(v)}{b_{\text{min}}^2 + b_{\text{gr}}^2(v)}} + 12786v^2 \left(\frac{1 - 0.096v^3}{1 + 1844v^{1.62}} \right).$$

DM distribution function in velocity space.— To better understand the distribution of velocities in the companion's frame, in Fig. 4 we show a density plot of the distribution function $dN/(dVd^3v^i)$ for a companion in a circular orbit⁶ at the ISCO radius. We show the region $v^1 \geq 0$ of a slice $v^2 = 0$, as the distribution function is symmetric under $v^1 \rightarrow -v^1$ (for equatorial orbits, it is also symmetric under $v_2 \rightarrow -v^2$).

The white region represents the loss cone of the DM spike, i.e., only particles with velocities within the colored regions are in stable bound orbits around the supermassive BH. All the others are either unbound or captured by the supermassive BH. We notice two disconnected regions associated with DM particles in prograde and retrograde motion relative to the companion orbit. For a companion in circular orbit at large radii, the prograde region is roughly centered at $v^3 = 0$, while for orbital radii in the strong-field, most prograde orbits have $v^3 < 0$, contributing a net positive torque to the EMRI. Simplified models that neglect the velocity anisotropy of the distribution cannot capture the radius-dependent competition between positive and negative torques, which can

⁵ We used $\delta\tau_{\text{int}} \lesssim x_H/|v^3|$, assuming $\langle \mathcal{L}_z \rangle \approx 0$; but the argument holds as long as $|v^3| \sim |l_z|/R$.

⁶ Or at pericenter or apocenter.

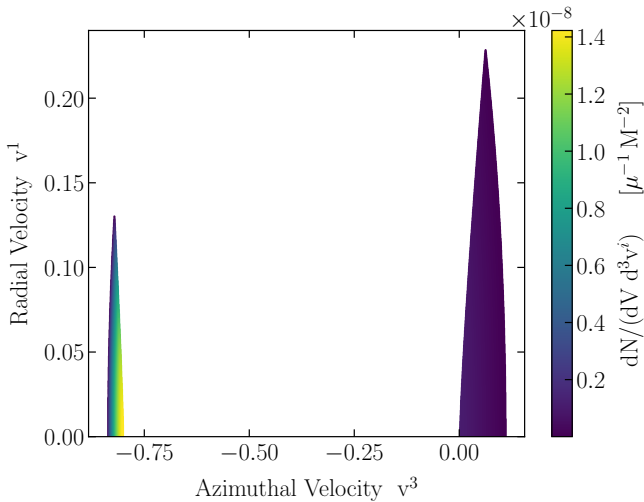


FIG. 4. **Distribution function in the companion frame at the ISCO ($R = 6M$) for the region $v^1 \geq 0$ of a slice $v^2 = 0$.** For a (quasi)circular EMRI, the distribution function is symmetric under $v^1 \rightarrow -v^1$. The white region shows the loss cone of our fiducial DM spike; only the velocities in the colored regions correspond to stable bound orbits around the supermassive BH.

affect the final torque. In fact, when using the distribution function $dN/(dV d^3v^i)$ as measured by the stationary observers [$\mathbf{n} = (-g_{tt})^{-1/2} \partial_t$] in the integration in Eq. (7), we observe a change of sign in the friction force happening at $r \approx 8M$ (close to the peak density). Thus, the ‘friction’ effectively becomes an ‘impulse’ at smaller radii than $8M$. We have also checked that the same happens for a Newtonian computation with Gondolo-Silk spike [75]; in that case, the transition happens at a larger radius $r \approx 15M$ (again near the peak density).

As explained in the text, both in the Newtonian and phenomenological (with heuristic relativistic effects) models, we used the distribution function perceived by stationary observers $\mathbf{n} = (-g_{tt})^{-1/2} \partial_t$ to evaluate the integral in d^3v^i . Their different local plane of

simultaneity changes the distribution function relatively to the companion’s (shown in Fig. 4 for $R = 6M$) by a multiplicative factor $(-g_{tt})^{-1/2} \mathcal{E}/\gamma_v$, while not changing the loss cone. This implies that these observers perceive a considerably smaller density of particles in retrograde orbits and slightly larger in prograde orbits.

Comparison between different models.— In Fig. 5, we compare the faithfulness between multiple models as a function of observation period. The oscillations are due to the incidental interference for long waveforms and do not carry any physical meaning (see, e.g., [54]). We show that the Newtonian and phenomenological models (with heuristic relativistic effects) can largely underestimate the impact of environmental effects on GW waveforms. It is also shown that relativistic corrections to interaction with the environment are comparatively weaker for systems with less extreme mass ratios, as such systems chirp faster through the strong-field region.

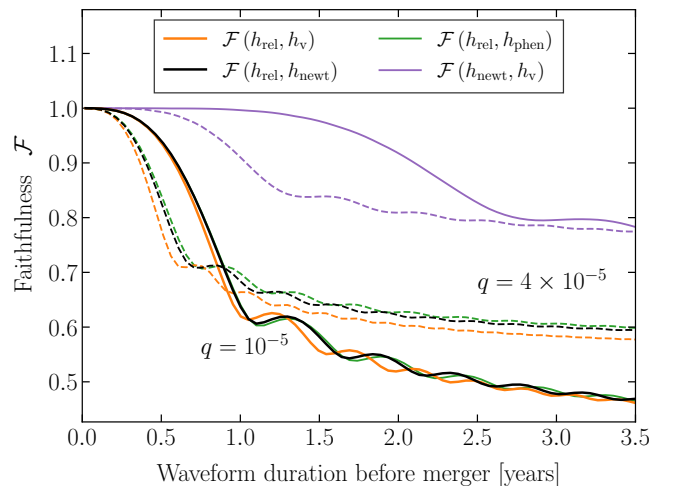


FIG. 5. **Faithfulness between different models as a function of signal duration (in years before merger).** The solid lines are for the benchmark $q = 10^{-5}$ system, while the dashed are for a slightly heavier companion.